Acta Crystallographica Section A
Foundations of Crystallography
ISSN 0108-7673

Received 20 October 2005
Accepted 15 November 2005

Reciprocal-space mapping of epitaxic thin films with crystallite size and shape polydispersity

A. Boulle,* F. Conchon and R. Guinebretière

Science des Procédés Céramiques et de Traitements de Surface, CNRS UMR 6638, ENSCI, 47-73 Avenue Albert Thomas, 87065 Limoges CEDEX, France. Correspondence e-mail: a_boulle@ensci.fr

A development is presented that allows the simulation of reciprocal-space maps (RSMs) of epitaxic thin films exhibiting fluctuations in the size and shape of the crystalline domains over which diffraction is coherent (crystallites). Three different crystallite shapes are studied, namely parallelepipeds, trigonal prisms and hexagonal prisms. For each shape, two cases are considered. Firstly, the overall size is allowed to vary but with a fixed thickness/width ratio. Secondly, the thickness and width are allowed to vary independently. The calculations are performed assuming three different size probability density functions: the normal distribution, the lognormal distribution and a general histogram distribution. In all cases considered, the computation of the RSM only requires a two-dimensional Fourier integral and the integrand has a simple analytical expression, *i.e.* there is no significant increase in computing times by taking size and shape fluctuations into account. The approach presented is compatible with most lattice disorder models (dislocations, inclusions, mosaicity, ...) and allows a straightforward account of the instrumental resolution. The applicability of the model is illustrated with the case of an yttria-stabilized zirconia film grown on sapphire.

© 2006 International Union of Crystallography
Printed in Great Britain – all rights reserved

1. Introduction

X-ray diffractometry (XRD), and especially reciprocal-space mapping, are widely used for the analysis of the structural characteristics of epitaxic thin films. The quantitative comparison of calculated reciprocal-space maps (RSMs) with experimental data allows one to obtain a detailed description of the defect structure, for instance in terms of dislocations (Holý *et al.*, 1995; Kaganer *et al.*, 1997), inclusions (Nesterets & Punegov, 2000) or mosaicity (Holý *et al.*, 1994). In that type of study, attention is primarily focused on the determination of the nature and the density of the defects present in the film, with little or no consideration for size effects induced by the finite extension (mainly in the in-plane direction) of the crystallites[1] building up the film. This is justified as long as the aforementioned size effects are negligible compared with lattice disorder effects induced by the defects, say for crystallite sizes larger than a few hundred nanometres. In such a case, size effects can be either neglected (*i.e.* one assumes laterally infinite crystallites) or accounted for by using crude descriptions of the crystallite shape, *e.g.* spheres or parallelepipeds with edges parallel to the diffraction plane.

However, with the ever-growing interest in nanostructured crystalline materials, size effects become prominent, so that the obtaining of reliable information concerning the defect structure of thin films requires an accurate description of the crystallite shape. Moreover, the determination of the actual shape of the crystallites is a fundamental task by itself since the shape of the crystallites significantly affects the properties of nanostructured materials (Gleiter, 2000). In this field, the most significant developments have been achieved for laterally patterned semiconductor nanostructures (Pietsch *et al.*, 2004; Schmidbauer, 2004), which exhibit a high degree of size and shape regularity. Most thin-film systems, however, especially imperfect thin films, exhibit a more or less pronounced degree of size and shape polydispersity that drastically affects the intensity distribution (mainly by suppressing interference fringes). Hence, besides the determination of size distributions by XRD, which constitutes an important task by itself, the analysis of strain in thin films also requires a careful account of size and shape fluctuations. An important issue on the way is that a complete two-dimensional intensity distribution has to be calculated for each crystallite size (and/or shape) and these distributions have then to be added according to a given probability density function (PDF), which obviously results in increased computing times. The importance of this effect for the study of strain in thin films (especially imperfect thin films) has been pointed out recently, either by using an approximate treatment involving two crystallite sizes (Kirste *et al.*, 2005) or by using a complete size distribution but with an analysis restricted to one-dimensional profiles (Boulle *et al.*, 2003; Boulle, Guinebretière, Masson *et al.*, 2005).

[1] Throughout the paper, the term crystallite is used to designate the crystalline domains over which diffraction is coherent, *i.e.* the amplitudes are added. Between different crystallites, the intensities are added.

In this work, we present a new development that allows size and shape fluctuations to be readily taken into account in the simulation of RSMs without requiring additional lengthy numerical evaluations compared with the ideal case with regular size and shape. The paper is organized as follows. In §2, we briefly recall the basic equations of the kinematical theory of diffraction from epitaxic thin films. In §3, the influence of particular crystallite shapes on RSMs is discussed, and, in §§4 and 5, we address the effects of size and shape fluctuations. In the last section, the compatibility of our approach with existing defect models is discussed, and its applicability is tested using an example related to recent experiments on yttria-stabilized zirconia films grown on sapphire.

2. X-ray diffraction from thin films

In the following, the derivation is carried out in the framework of the kinematical theory of diffraction, which is justified for nanostructured materials studied at non-grazing angles (Pietsch *et al.*, 2004). This assumption also ensures the compatibility of our approach with many existing models of lattice disorder, which in general make use of the kinematical approximation (Holý *et al.*, 1994; 1995; Kaganer *et al.*, 1997, 2005; Nesterets & Punegov, 2000). Moreover, this theory allows an easier handling of the expression of the diffracted intensity than the, though more rigorous, dynamical theory (Authier, 2005). For simplicity, as often assumed in similar studies, we neglect the scattering from the substrate. If this assumption turns out to be unjustified, then the contribution of the substrate must be taken into account either by adding the amplitudes, if the film and substrate scatter coherently, or by adding the intensities in the opposite case. With this simplification, the intensity diffracted in the vicinity of the reflection with reciprocal-lattice vector $\mathbf{h}$ reads (Pietsch *et al.*, 2004)

$$I(\mathbf{q}) = \int\int \mathrm{d}\mathbf{r}\,\mathrm{d}\Delta\mathbf{r}\,\Omega(\mathbf{r})\Omega(\mathbf{r}+\Delta\mathbf{r})\exp\{i\mathbf{h}[\mathbf{u}(\mathbf{r}+\Delta\mathbf{r})-\mathbf{u}(\mathbf{r})]\}\\ \times \exp(i\mathbf{q}\Delta\mathbf{r}),$$

where $\mathbf{u}(\mathbf{r})$ is the lattice displacement at the point $\mathbf{r}$, $\Delta\mathbf{r}$ is a vector joining two points $\mathbf{r}$ and $\mathbf{r}'$ in the film, $\mathbf{q}$ is the deviation of the scattering vector $\mathbf{Q}$ from the Bragg position ($\mathbf{q} = \mathbf{Q} - \mathbf{h}$) and $\Omega(\mathbf{r})$ is the crystallite shape function. $\Omega(\mathbf{r})$ describes the shape of the crystalline domains over which diffraction is coherent, *i.e.* $\Omega(\mathbf{r}) = 1$ within a domain and $\Omega(\mathbf{r}) = 0$ outside. In the case of continuous films, which are in general built of grains separated by grain boundaries, $\Omega(\mathbf{r})$ can safely be considered as the grain shape function. In the case of discontinuous (islanded) films, $\Omega(\mathbf{r})$ can be considered as the island shape function only if different islands diffract incoherently, otherwise $\Omega(\mathbf{r})$ must contain information concerning both the island shape and the spatial distribution of the islands. In the present study, we are mainly interested in imperfect thin-film systems, we shall therefore not consider the latter case. As mentioned earlier, specific treatments have been developed for high-quality laterally patterned nanostructures (Pietsch *et al.*, 2004; Schmidbauer, 2004), this point is therefore out of the scope of this paper. Let us first assume a statistically homogeneous sample (we discuss this assumption in §6). In such a case, the choice of the origin is unimportant and the exponential involving $\mathbf{u}(\mathbf{r})$ can be replaced by its statistical average performed over the defect distribution,

$$G(\Delta\mathbf{r}) = \langle\exp\{i\mathbf{h}[\mathbf{u}(\Delta\mathbf{r}) - \mathbf{u}(0)]\}\rangle. \tag{1}$$

In the following, we conform to the usual terminology and refer to $G(\Delta\mathbf{r})$ as the pair correlation function. The integral over $\mathbf{r}$ hence only implies $\Omega(\mathbf{r})$ and can be written $V(\Delta\mathbf{r}) = \Omega(\Delta\mathbf{r}) * \Omega(-\Delta\mathbf{r})$, which is the autocorrelation function of $\Omega(\mathbf{r})$ ($*$ denotes the convolution operator). We shall refer to $V(\Delta\mathbf{r})$ as the correlation volume. Throughout the paper, we adopt the common notation where the z axis is chosen perpendicular to the film surface, the x axis is parallel to the projection of the incident beam in the film plane and the y axis is chosen perpendicular to the plane defined by x and z (the diffraction plane). We now take into account the fact that in most X-ray diffractometers the beam is not collimated perpendicularly to the diffraction plane. The expression for the diffracted intensity must hence be integrated over q_y, which gives rise to the delta function $\delta(y)$. We then obtain

$$I(q_x, q_z) = \int\int \mathrm{d}x\,\mathrm{d}z\,V(x,0,z)\langle\exp\{i\mathbf{h}[\mathbf{u}(x,0,z) - \mathbf{u}(0,0,0)]\}\rangle_y\\ \times \exp[i(q_x x + q_z z)], \tag{2}$$

where x, y, z are the components of the vector $\Delta\mathbf{r}$ and the subscript y indicates that the average has to be performed in all planes with equation $y = 0$. We show below that the effect of size and shape polydispersity can be simply accounted for by replacing the correlation volume $V(x,0,z)$ with an averaged correlation volume $\langle V(x,0,z)\rangle$ that can be calculated analytically in many relevant cases, *i.e.* there is no need for additional numerical integrations. We now return to equation (2) and evaluate the correlation volume for a simple case, namely a parallelepiped with edges parallel to the diffraction plane and with dimensions $X \times Y \times Z$. We directly obtain the well known result $V(x,y,z) = (X - |x|)(Y - |y|)(Z - |z|)$. When $y = 0$, the intensity is proportional to Y, *i.e.* it is proportional to the number of lattice planes in the y direction so that in the scattering process the sample can be considered as being divided into (x, z) lattice planes that diffract incoherently with respect to each other. This is analogous to the 'column model' referred to in powder diffraction (Warren, 1969). Because of a two-dimensional integration perpendicular to $\mathbf{Q}$, in powder diffraction one speaks of columns instead of planes. It should be noticed that in the field of powder diffraction the integration arises because of the random orientation of the crystallites, whereas in the present case the integration arises from a lack of resolution in the direction perpendicular to the diffraction plane. This approach is correct only if the divergence of the scattered radiation is much smaller than the divergence of the incident beam (and/or the acceptance of the detector), for instance if the mosaicity is much smaller than the divergence of the incident beam. This is actually the case for most thin-film systems studied on laboratory X-ray diffractometers. However, even in the case of thin films

Table 1
Values of the coefficients b_n and the parameter k for parallelepipeds.

The notation $\phi[x]$ means ϕ modulo x. α is the in-plane aspect ratio of the parallelepiped, *i.e.* $\alpha = D_y/D_x$.

	$\phi[\pi] \leq \pi/2$	$\phi[\pi] > \pi/2$
b_2	α	α
b_1	$-x(\alpha \cos \phi + \sin \phi)$	$-x(\alpha \sin \phi + \cos \phi)$
b_0	$x^2 \cos \phi \sin \phi$	$x^2 \cos \phi \sin \phi$

	$\phi \leq \mathrm{atan}(\alpha)$	$\phi > \mathrm{atan}(\alpha)$	$\phi \leq \pi - \mathrm{atan}(\alpha)$	$\phi > \pi - \mathrm{atan}(\alpha)$
k	$1/\cos \phi$	$\alpha/\sin \phi$	$\alpha/\cos \phi$	$1/\sin \phi$

exhibiting a mosaicity larger than the divergence of the incident beam, the q_y integration is ensured by the angular disorientation of the crystallites (similarly to powder diffraction) and equation (2) is equally valid. Hence, the present approach does not hold only in the case of thin films exhibiting a very low mosaicity studied with an incident beam collimated perpendicularly to the diffraction plane, so that the q_y integration cannot be ensured.

A geometrical interpretation of the correlation volume is shown in Fig. 1. The correlation volume corresponds to the common volume between a crystallite and the same crystallite shifted by $\Delta\mathbf{r}$. In the field of powder diffraction, this is known

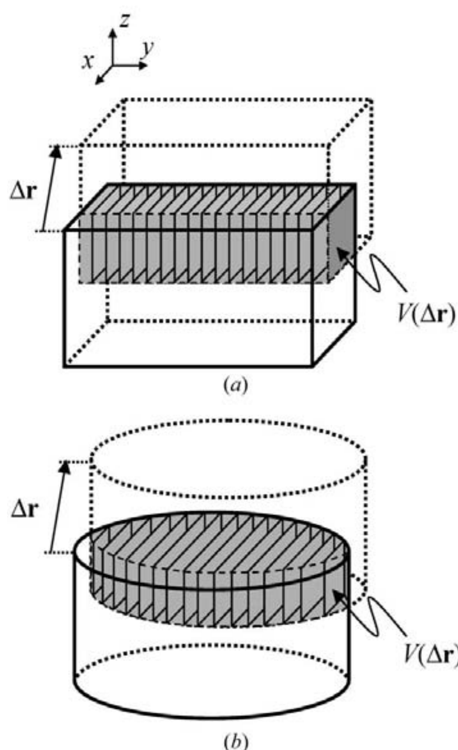

Figure 1
(*a*) Correlation volume for a parallelepiped with a correlation vector $\Delta\mathbf{r}$. Because of the lack of resolution in the y direction, the correlation volume is 'divided' into lattice planes diffracting incoherently and parallel to the (x, z) plane. Moreover, $\Delta\mathbf{r}$ is constrained to lie in the (x, z) plane. (*b*) Same as (*a*) for a cylindrical shape. The lattice planes now have different sizes.

Table 2
Values of the coefficients b_n and the parameter k for trigonal prisms.

The notation $\phi[x]$ means ϕ modulo x.

	$\phi[\pi/3] \leq \pi/6$	$\phi[\pi/3] > \pi/6$
b_2	$3^{1/2}/4$	$3^{1/2}/4$
b_1	$-x \sin(\pi/2 - \phi[\pi/3])$	$-x \sin(\pi/6 + \phi[\pi/3])$
b_0	$x^2 \sin^2(\pi/2 - \phi[\pi/3])/3^{1/2}$	$x^2 \sin^2(\pi/6 + \phi[\pi/3])/3^{1/2}$
k	$3^{1/2}/(2 \cos \phi[\pi/3])$	$\cos(\phi[\pi/3] - \pi/6)$

Table 3
Values of the coefficients b_n and the parameter k for hexagonal prisms.

The notation $\phi[x]$ means ϕ modulo x.

	$x \leq D3^{1/2}/(\cos \phi[\pi/3] + 3^{1/2} \sin \phi[\pi/3])$	$x > D3^{1/2}/(\cos \phi[\pi/3] + 3^{1/2} \sin \phi[\pi/3])$
b_2	$3 \times 3^{1/2}/2$	$2 \times 3^{1/2}$
b_1	$-2x \cos \phi[\pi/3]$,	$-x3^{1/2}(\sin \phi[\pi/3] + 3^{1/2} \cos \phi[\pi/3])$
b_0	$-x^2 3^{1/2}\{\sin^2\phi[\pi/3] - (1/3) \cos^2\phi[\pi/3]\}/2$	$x^2 \cos \phi[\pi/3](\cos \phi[\pi/3] + 3^{1/2} \sin \phi[\pi/3])/3^{1/2}$

	$\phi[\pi/3] \leq \pi/6$	$\phi[\pi/3] > \pi/6$	$\phi[\pi/3] \leq \pi/6$	$\phi[\pi/3] > \pi/6$
k	$3^{1/2}/\cos \phi[\pi/3]$	$2 \cos(\phi[\pi/3] - \pi/6)$	$3^{1/2}/\cos \phi[\pi/3]$	$2 \cos(\phi[\pi/3] - \pi/6)$

as the 'ghost' concept (James, 1967). In powder diffraction, $\Delta\mathbf{r}$ is necessarily collinear to $\mathbf{Q}$, whereas in the present case it can lie along any direction in the (x, z) plane. The intensity is then obtained by adding the intensities of all (x, z) planes contained in the correlation volume and for all possible correlation volumes. For a differently oriented crystallite, or for crystallites with a different shape (Fig. 1*b*), the planes contained in the correlation volume will exhibit different sizes. It can be expected that this will affect the diffracted intensity. We discuss this point in the next section.

3. The correlation volume of common shapes

The grains building up thin films are in general highly anisotropic. Their description hence requires at least two-dimensional parameters: an in-plane (IP) dimension, D, and an out-of-plane (OOP) dimension, t, which we shall write as a function of the grain aspect ratio f, $t = fD$. If diffraction is coherent across the film thickness, t corresponds to the film thickness, otherwise t simply corresponds to the crystallite size in the OOP direction. With these definitions, it turns out that the correlation volume of many experimentally relevant cases can be written as a polynomial of third degree, $a_3D^3 + a_2D^2 + a_1D + a_0$, where the coefficients a_n are functions of the crystallite shape, of the coordinates x, y, z and of the orientation (defined by the angle ϕ) of the crystallite with respect to the diffraction plane. For instance, for spherical crystallites with diameter D, $a_3 = \pi/6$, $a_2 = -\pi(x^2 + z^2)^{1/2}/4$, $a_1 = 0$ and $a_0 = \pi(x^2 + z^2)^{3/2}/12$ (Pietsch *et al.*, 2004). We shall assume that the grains exhibit a flat top and vertical sides. In principle, this assumption is not necessary, but it indeed corresponds to a case frequently encountered in practice and it will also simplify the discussion

in §6 where samples exhibiting two-dimensional statistical homogeneity will be considered. The shape factor can then be written $\Omega(x,y,z) = \Omega(x,y)\Omega(z)$ and the correlation volume can hence be written as a product of two polynomials, $(b_2D^2 + b_1D + b_0)(c_1D + c_0)$. Since the crystallites are flat, it is obvious that $c_1D + c_0 = t - |z|$ for $|z| \leq t$ and 0 otherwise, which corresponds to the Fourier transform of $t^2\mathrm{sinc}^2(q_zt/2)$. The b_n coefficients depend on the IP crystallite shape, the coordinate x and the angle ϕ. We derived the expression for the correlation volume of parallelepipeds, trigonal prisms and hexagonal prisms. The corresponding expressions for the b_n coefficients are given in Tables 1–3 [for hexagonal prisms, details can also be found in Vargas *et al.* (1983)]. The expression of the correlation volume can be derived geometrically for other experimentally relevant cases using the ghost concept.

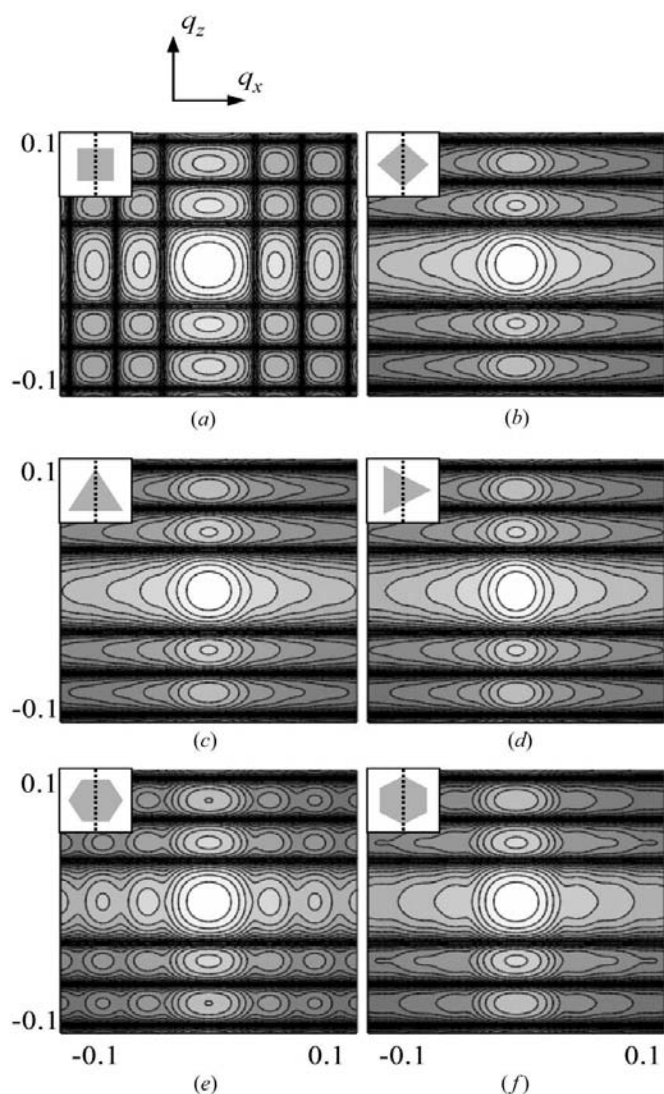

Figure 2
Calculated RSMs for different crystallite shapes and orientations. (*a*) Square parallelepiped with angle relative to the diffraction plane $\phi = 0$. (*b*) Square parallelepiped with $\phi = 45^\circ$. (*c*) Trigonal prism with $\phi = 0$. (*d*) Trigonal prism with $\phi = 30^\circ$. (*e*) Hexagonal prism with $\phi = 0$. (*f*) Hexagonal prism with $\phi = 30^\circ$. All crystallites have the same volume ($20 \times 20 \times 20$ nm^3) and the same height. In each figure, the inset represents the in-plane orientation of the crystallite with respect to the diffraction plane (marked as a dotted line).

The RSMs associated with the corresponding shapes can be calculated using equation (2). In principle, the bounds of the integral are $\pm\infty$. However, since the correlation volume drops to zero above particular values of x and z (this can be straightforwardly understood from Fig. 1), for practical purposes it is useful to use those finite bounds. In the OOP direction, this bound is equal to the thickness t, whereas in the IP direction it depends both on the crystallite size and the angle ϕ, and we shall denote that bound kD (the corresponding values of k are given in Tables 1–3). Computed RSMs are shown in Fig. 2 for each of the considered shapes and for two different orientations ϕ. All crystallites have the same volume $20 \times 20 \times 20$ nm^3 and the same thickness. In the OOP direction, the thickness (interference) fringes of the sinc^2 function are clearly visible and are obviously independent of the IP orientation. In the IP direction, perfect sinc^2 fringes are only visible for the parallelepiped when $\phi = 0$, *i.e.* when the parallelepiped is parallel to the diffraction plane. For all other orientations or crystallite shapes, the fringe structure is profoundly affected by the size variation of the (x,z) lattice planes (Fig. 1*b*). Fringes are still visible for the hexagonal prism at $\phi = 0$, but they are almost completely absent for the other cases. The lack of fringes hence does not necessarily imply the existence of lattice disorder or fluctuations of the crystallite size. It may simply be induced by the shape of the crystallites. We now investigate the effects of size fluctuations.

4. Influence of size fluctuations

4.1. Averaged correlation volume

When the size of the domains over which diffraction is coherent is allowed to vary, the total diffracted intensity results from the addition of the intensities diffracted by different domains. This is written

$$I(q_x,q_z) = \int_0^\infty \mathrm{d}D\, p(D) \int_{-kD}^{kD} \int_{-fD}^{fD} \mathrm{d}x\, \mathrm{d}z V(x,0,z)G(x,0,z) \times \exp[i(q_xx + q_zz)], \quad (3)$$

where $p(D)$ is the PDF of the variable D. We now change the order of integration and assume that the pair correlation function $G(x,0,z)$ is independent of the crystallite size (we discuss this assumption in §6). We obtain

$$I(q_x,q_z) = \int_{-\infty}^{\infty} \int_{-\infty}^{\infty} \mathrm{d}x\, \mathrm{d}z\, \langle V(x,0,z)\rangle G(x,0,z) \exp[i(q_xx + q_zz)] \quad (4a)$$

and

$$\langle V(x,0,z)\rangle = \int_{D_{\min}}^{\infty} \mathrm{d}D\, p(D)V(x,0,z). \quad (4b)$$

Equation (4) is equivalent to equation (2) except that the correlation volume is replaced by an averaged correlation

volume. Equation (4) can be qualitatively interpreted as follows: for a given correlation vector (*i.e.* given x and z), add the intensities of all (x, z) planes contained in the correlation volume, but contrary to equation (2), where this summation is restricted to one crystallite, in equation (4), the planes contained in different crystallites must be considered. However, a crystallite with dimensions D or t smaller than x/k or z/f, respectively, cannot contain a particular (x, z) plane. An obvious example is a parallelepiped with IP dimension $D < x$: it cannot contain a particular (x, z) plane, even if $t > z$. The lower bound in equation (4*b*) is therefore $D_{\min} = \max(x/k, z/f)$. With the polynomial defined in the previous section, the averaged correlation volume can finally be written

$$\langle V(x, 0, z)\rangle = \sum_{n=0}^{3} a_n \int_{D_{\min}}^{\infty} \mathrm{d}D\, p(D) D^n. \qquad (5)$$

4.2. Size distributions

The integral in equation (5) can be evaluated analytically for many experimentally relevant cases. In the following, we shall consider the normal (Gaussian) and the lognormal distributions, which are broadly used in practice to model size distributions in nanocrystalline systems. These functions are defined as follows: for the Gaussian with mean μ and variance σ^2,

$$p_N(D) = \frac{1}{(2\pi)^{1/2}\sigma} \exp\left[-\tfrac{1}{2}\left(\frac{D-\mu}{\sigma}\right)^2\right]$$

and for the lognormal distribution with lognormal mean $\mu_{\rm LN}$ and variance $\sigma_{\rm LN}^2$,

$$p_{\rm LN}(D) = \frac{1}{(2\pi)^{1/2} D \sigma_{\rm LN}} \exp\left[-\tfrac{1}{2}\left(\frac{\ln D - \mu_{\rm LN}}{\sigma_{\rm LN}}\right)^2\right].$$

The parameters $\mu_{\rm LN}$ and $\sigma_{\rm LN}$ are related to μ and σ by $\mu = \exp(\mu_{\rm LN} + \sigma_{\rm LN}^2/2)$ and $\sigma^2 = \exp(2\mu_{\rm LN} + \sigma_{\rm LN}^2)[\exp(\sigma_{\rm LN}^2) - 1]$. However, these functions may fail to correctly describe particular distributions (for instance bimodal distributions), so we shall therefore also consider histogram distributions (Fig. 3) which can be directly obtained by complementary imaging techniques (*e.g.* atomic force microscopy, or transmission or scanning electron microscopy). It is worth noticing that the Gaussian distribution must be used carefully. Indeed, for a mean size μ smaller than 3σ, negative sizes occur in the distribution. To avoid this, the Gaussian distribution has to be constrained with the condition $\sigma < \mu/3$. After straightforward but tedious calculations, the averaged correlation volume follows, for the Gaussian PDF,

$$\begin{aligned}\langle V(x, 0, z)\rangle = {} & \tfrac{1}{2}\operatorname{erfc}\left(\frac{D_{\min}-\mu}{2^{1/2}\sigma}\right)[a_3(\mu^3 + 3\mu\sigma^2) + a_2(\mu^2+\sigma^2) \\ & + a_1\mu + a_0] + \frac{\sigma}{(2\pi)^{1/2}}\exp\left[-\tfrac{1}{2}\left(\frac{D_{\min}-\mu}{\sigma}\right)\right] \\ & \times [a_3(D_{\min}^2 + \mu D_{\min} + \mu^2 + 2\sigma^2) \\ & + a_2(D_{\min}+\mu) + a_1],\end{aligned}$$

and, for the lognormal PDF [a similar equation was given in the field of powder diffraction by Scardi & Leoni (2001)],

$$\begin{aligned}\langle V(x, 0, z)\rangle = {} & \tfrac{1}{2}\sum_{n=0}^{3} a_n \exp\left(n\mu_{\rm LN} + n^2\frac{\sigma_{\rm LN}^2}{2}\right) \\ & \times \operatorname{erfc}\left(\frac{\ln D_{\min} - \mu_{\rm LN} - n\sigma_{\rm LN}^2}{2^{1/2}\sigma_{\rm LN}}\right).\end{aligned}$$

For the histogram distribution defined in Fig. 3, we obtain

$$\langle V(x, 0, z)\rangle = \sum_{m=0}^{M}(p_m - p_{m+1})\sum_{n=0}^{3}\frac{a_n}{n+1}D_m'^{n+1},$$

where M is the number of size classes and $D_m' = \max(D_m, D_{\min})$. The following constraints are needed: $p_0 = p_{M+1} = 0$ and $p_{i<m} = 0$ if $D_m < D_{\min}$.

Calculated RSMs for increasing size fluctuations are shown in Fig. 4. The effects of a size distribution on the RSM is more easily evidenced with a parallelepipedic crystallite shape, we therefore only show the results for this particular case. However, similar effects are observed for other shapes. When the variance increases, the most striking feature is the broadening of the thickness fringes in the radial direction with respect to the centre of the reciprocal-lattice point. The broadening is more pronounced for large deviations from the Bragg position so that high-order fringes are completely smeared out for increasing σ (Figs. 4*b*, *c*). For high values of σ (Figs. 4*c*, *d*), the fringes are completely damped and the main peak is significantly narrower than for $\sigma = 0$. The calculation is here performed for a lognormal distribution of size. For not too large a variance (*i.e.* $\sigma < \mu/3$), the Gaussian and the lognormal distributions give very similar results. However, the lognormal is more versatile that the Gaussian since the latter is constrained to have $\sigma < \mu/3$ to avoid negative sizes, whereas the former, which is asymmetric, allows for much larger values of σ.

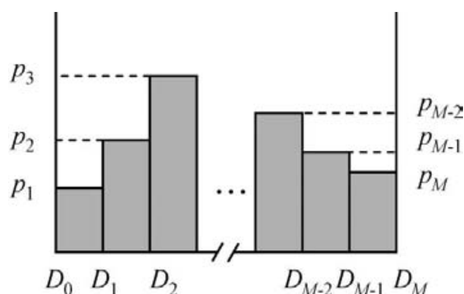

Figure 3
Histogram distribution, with M size classes and associated probabilities p_m.

5. Size and shape fluctuations

There are some cases where the above model, *i.e.* a single size distribution, is not sufficient to describe the microstructure of actual thin films. This is for instance the case of films subjected to post-deposition thermal annealing. Those films undergo significant IP grain growth, whereas OOP grain growth does

not occur (Thomson, 1990). For such films, the aspect ratio, $f = t/D$, is not constant and two distributions (IP and OOP) are needed to model the microstructure correctly. In equation (3), an integration over t must hence be added. Changing the order of integration, we obtain [assuming again that $G(x, 0, z)$ is independent of D and t]

$$I(q_x, q_z) = \int\limits_{-\infty}^{\infty} \int\limits_{-\infty}^{\infty} \mathrm{d}x\,\mathrm{d}z\, \langle V(x,0)\rangle \langle V(z)\rangle G(x, 0, z) \times \exp[i(q_x x + q_z z)] \quad (6a)$$

and

$$\langle V(x,0)\rangle = \int\limits_{x/k}^{\infty} \mathrm{d}D\, p(D) V(x, 0) \quad (6b)$$

$$\langle V(z)\rangle = \int\limits_{z}^{\infty} \mathrm{d}t\, p(t) V(z). \quad (6c)$$

As above, equations (6b) and (6c) can be solved analytically. We obtain for the Gaussian PDF

$$\langle V(x,0)\rangle = \tfrac{1}{2}\,\mathrm{erfc}\left(\frac{D_{\min} - \mu_D}{2^{1/2}\sigma_D}\right)[b_2(\mu_D^2 + \sigma_D^2) + b_1\mu_D + b_0] + \frac{\sigma_D}{(2\pi)^{1/2}} \exp\left[-\tfrac{1}{2}\left(\frac{D_{\min} - \mu_D}{\sigma_D}\right)\right] \times [b_2(D_{\min} + \mu_D) + b_1]$$

$$\langle V(z)\rangle = \tfrac{1}{2}\,\mathrm{erfc}\left(\frac{z - \mu_t}{2^{1/2}\sigma_t}\right)[c_1\mu_t + c_0] + \frac{\sigma_t}{(2\pi)^{1/2}} \exp\left[-\tfrac{1}{2}\left(\frac{z - \mu_t}{\sigma_t}\right)\right].$$

For the lognormal PDF, this becomes

$$\langle V(x,0)\rangle = \tfrac{1}{2}\sum_{n=0}^{2} b_n \exp\left(n\mu_{D,\mathrm{LN}} + n^2 \frac{\sigma_{D,\mathrm{LN}}}{2}\right) \times \mathrm{erfc}\left(\frac{\ln D_{\min} - \mu_{D,\mathrm{LN}} - n\sigma_{D,\mathrm{LN}}^2}{2^{1/2}\sigma_{D,\mathrm{LN}}}\right)$$

$$\langle V(z)\rangle = \tfrac{1}{2}\sum_{n=0}^{1} c_n \exp\left(n\mu_{t,\mathrm{LN}} + n^2 \frac{\sigma_{t,\mathrm{LN}}}{2}\right) \times \mathrm{erfc}\left(\frac{\ln D_{\min} - \mu_{t,\mathrm{LN}} - n\sigma_{t,\mathrm{LN}}^2}{2^{1/2}\sigma_{t,\mathrm{LN}}}\right).$$

For the histogram distribution, this becomes

$$\langle V(x,0)\rangle = \sum_{m=0}^{M}(p_m - p_{m+1}) \sum_{n=0}^{2} \frac{b_n}{n+1} D_m'^{n+1}$$

$$\langle V(z)\rangle = \sum_{m=0}^{M}(p_m - p_{m+1}) \sum_{n=0}^{1} \frac{c_n}{n+1} t_m'^{n+1}.$$

In the above expressions, μ_D and σ_D (μ_t and σ_t) refer to the mean and square root of the variance of the PDF of the IP dimension D (of the OOP dimension t).

Calculated RSMs are displayed in Fig. 5 with the same parameters as in Fig. 4. It appears that the fringe structure is highly sensitive to the simultaneous presence of size and shape fluctuations. Indeed, since there are two distributions acting independently in the IP and OOP directions, the fringes are now broadened along these directions instead of the radial direction. In particular, the inclined streak running parallel to the diagonal of the parallelepiped is completely absent in the present case. Calculated RSMs of thin films exhibiting anisotropic size fluctuations are displayed in Figs. 5(e) and 5(f). Fig. 5(e) corresponds to a film with significant ($\sigma = \mu/3$) OOP size

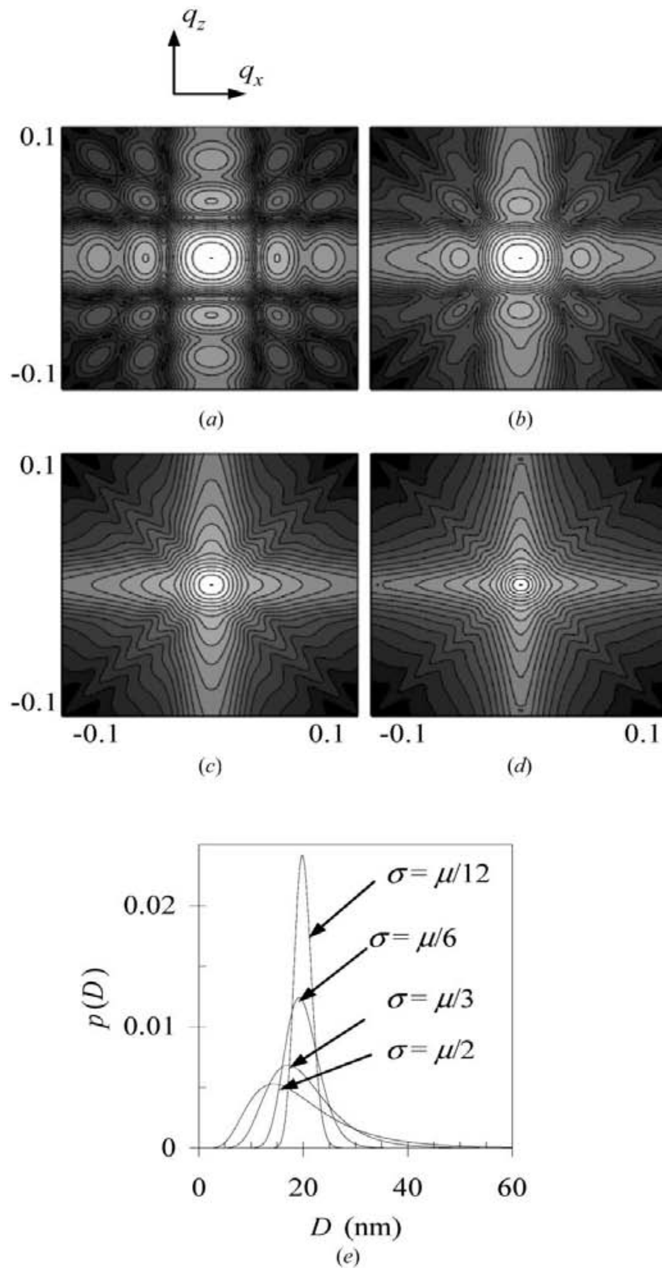

Figure 4
(a)–(d) Calculated RSMs of a film made of parallelepipedic crystallites lognormally distributed with average dimensions $\mu \times \mu \times \mu$ (μ = 20 nm) and increasing variance σ^2. (a) $\sigma = \mu/12$, (b) $\sigma = \mu/6$, (c) $\sigma = \mu/3$, (d) $\sigma = \mu/2$. (e) Corresponding size distributions. Increasing σ results in the broadening of the fringes in the radial direction with respect to the Bragg position $q_x = q_z = 0$. The broadening increases with increasing q_x and q_z, *i.e.* high-order fringes are more affected. For high σ values, the fringes are completely smeared out.

fluctuations and negligible IP fluctuations, whereas Fig. 5(*f*) corresponds to a significant IP size fluctuation and negligible OOP fluctuation. The latter case is expected to be particularly useful since actual RSMs often display pronounced thickness fringes in the OOP direction whereas no such fringes are observed in the IP direction.

All the above presented RSMs imply the computation of a two-dimensional Fourier integral, *i.e.* there is no significant increase in computing times by taking size and shape fluctuations into account. However, actual thin films not only exhibit size and shape fluctuations but they also exhibit lattice disorder. The approach presented here will be useful for practical use only if it is compatible with existing models of lattice disorder. We discuss this point in the following section.

6. Discussion and applications

In deriving the expression for the diffracted intensity of a thin film exhibiting crystallite size fluctuations [equation (4)] or size and shape fluctuations [equation (6)], two major assumptions were made. Firstly, three-dimensional statistical homogeneity is required, otherwise the diffracted intensity cannot be written as the Fourier transform of the product of two terms [one term containing information concerning crystallite size and shape, and the other term describing lattice disorder, equation (2)]. Secondly, the pair correlation function $G(x, 0, z)$ describing lattice disorder has to be independent of the crystallite size, otherwise the diffracted intensity cannot be written as the Fourier transform of the product of two terms [one term containing information concerning crystallite size and shape *and their fluctuations*, and the other term describing lattice disorder, equations (4) and (6)]. An important consequence of this last assumption is that the present approach does not account for correlations between the crystallite size and its state of disorder. If $G(x, 0, z)$ is indeed dependent on the crystallite size then equation (3) has to be evaluated numerically, which obviously results in increased computing times.

The first assumption implies that the defects are randomly distributed throughout the film volume. Disorder models fulfilling this condition were given for inclusions, dislocation loops and stacking faults [for a recent review, see Pietsch *et al.* (2004) and references therein] as well as for threading dislocations [for a recent review, see Kaganer *et al.* (2005) and references therein]. For these defects, it can be reasonably assumed that the second assumption is valid as long as the defect size is much smaller than the crystallite size (Pietsch *et al.*, 2004). An important model of defects is the well known mosaic block model. Although this model is in general only a rough approximation of the actual state of strain in thin films (compared to the aforementioned models), this model has proven to be particularly useful because of its straightforwardness, especially in the case of materials where the actual defect structure is not well known. It is useful to express the mosaicity in terms of the components of the heterogeneous strain tensor (Ratnikov *et al.*, 2000), $(\varepsilon_{xz} - \varepsilon_{zx})/2$, which we shall write as $\varepsilon_{zx}^{(M)}$, where the superscript M stands for mosaicity. The symmetric part of the heterogeneous strain tensor, $(\varepsilon_{xz} + \varepsilon_{zx})/2$, corresponds to shear strain, which we shall denote as $\varepsilon_{zx}^{(S)}$. The statistical average in equation (1) is often performed in the framework of the central limit theorem, *i.e.* assuming a Gaussian PDF. However, the Gaussian distribution is known to fail in some cases (Boulle, Guinebretière & Dauger, 2005), and in particular it is unable to account for XRD profiles exhibiting power-law-type tails. We recently suggested the use of Lévy-stable distributions to perform this average (Boulle, Guinebretière, Masson *et al.*, 2005; Boulle, Guinebretière & Dauger, 2005). Lévy-stable distributions arise in the framework of the *generalized* central limit theorem (Feller, 1970) and they are in general defined using their characteristic function, $\langle \exp(ikr) \rangle$, where r and k are real- and

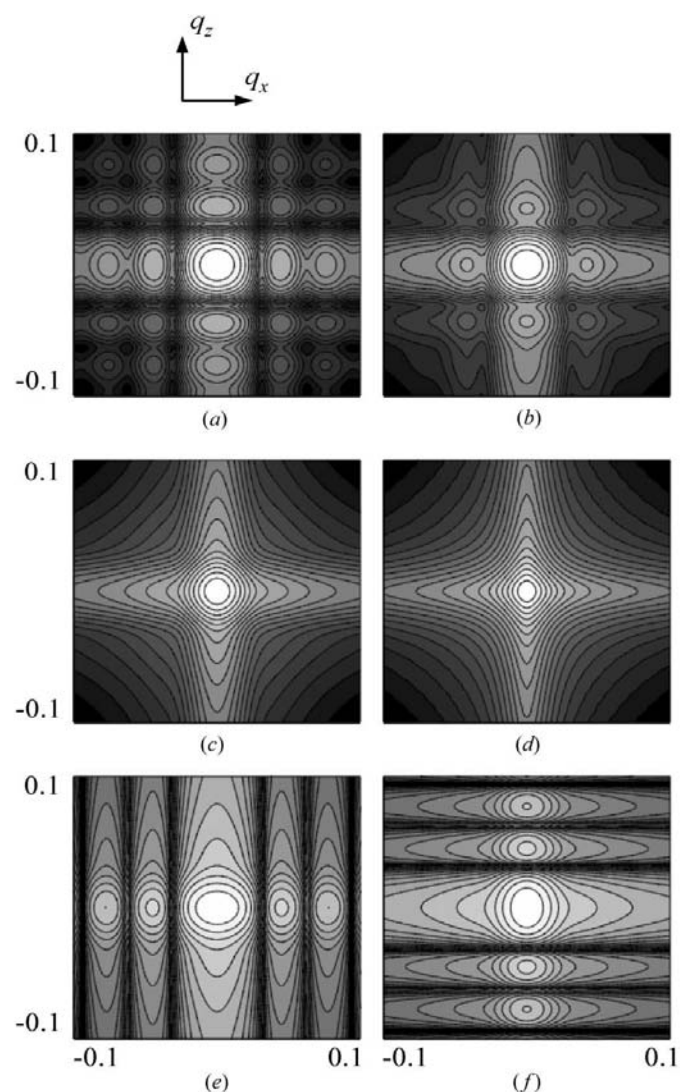

Figure 5
(*a*)–(*d*) Calculated RSMs of a film made of parallelepipedic crystallites lognormally distributed with average dimensions $\mu_D \times \mu_D \times \mu_t$ ($\mu_D = \mu_t = 20$ nm) and increasing variance σ_D^2 and σ_t^2. (*a*) $\sigma_D = \sigma_t = \mu/12$, (*b*) $\sigma_D = \sigma_t = \mu/6$, (*c*) $\sigma_D = \sigma_t = \mu/3$, (*d*) $\sigma_D = \sigma_t = \mu/2$, (*e*) $\sigma_D = \mu/12$ and $\sigma_t = \mu/3$, (*f*) $\sigma_D = \mu/3$ and $\sigma_t = \mu/12$. Increasing σ results in the broadening of the fringes parallel to q_x and q_z. The broadening increases with increasing q_x and q_z, *i.e.* high-order fringes are more affected. For high σ values, the fringes are completely smeared out.

reciprocal-space variables, respectively. For symmetrical Lévy-stable distributions, it turns out that (Nolan, 1998)

$$\langle \exp(ikr) \rangle = \exp(i\mu k) \exp(-\tfrac{1}{2}\sigma^{\gamma}|k|^{\gamma})$$

where $\mu \in]-\infty, \infty[$ is the mode of the distribution, $\sigma \in [0, \infty[$ is the characteristic width (for instance it corresponds to the square root of the variance of the Gaussian distribution or to the full width at half-maximum of the Lorentzian distribution) and $\gamma \in]0, 2]$ is the tail index that defines the tail behaviour of the distribution (for instance $\gamma = 2$ for the Gaussian distribution, $\gamma = 1$ for the Lorentzian distribution). The case of general Lévy-stable distributions (*i.e.* asymmetrical distributions) has been presented elsewhere (Boulle, Guinebretière, Masson *et al.*, 2005). With this definition and assuming that the components of the strain tensor are statistically independent, the correlation function can be written

$$\begin{aligned} G(x, 0, z) = {}& \exp\{i[\bar{e}_{xx}h_x x + \bar{e}_{zz}h_z z + \bar{e}_{xz}^{(S)}(h_x z + h_z x) \\ & + \bar{e}_{xz}^{(M)}(h_x z - h_z x)]\} \exp\{-\tfrac{1}{2}[\varepsilon_{xx}^{\gamma}|h_x x|^{\gamma} + \varepsilon_z^{\gamma}|h_z z|^{\gamma} \\ & + \varepsilon_{xz}^{(S)\gamma}|h_x z + h_z x|^{\gamma} + \varepsilon_{xz}^{(M)\gamma}|h_x z - h_z x|^{\gamma}]\}, \end{aligned} \tag{7}$$

where $\bar{e}_{ij}$ are the components of the homogeneous strain tensor (which correspond to the mode of the PDF of the strain e_{ij}) and ε_{ij} are the components of the heterogeneous strain tensor (which correspond to the characteristic width of the PDF of the strain e_{ij}). For the Gaussian PDF ($\gamma = 2$), one obtains the same result as in Holý *et al.* (1995). This expression of $G(x, 0, z)$ can be used in combination with equations (4) or (6) to model RSMs of imperfect materials.

The case of misfit dislocations, which is of primary importance in the study of thin-film structures, does not fulfil both of the above-mentioned assumptions. Indeed, in such a case, straight dislocations parallel to a particular crystallographic direction are randomly distributed at the film/substrate interface so that statistical homogeneity can only be assumed in the IP direction. Moreover, the displacement field associated with misfit dislocations strongly depends on the film thickness (Kaganer *et al.*, 1997) and therefore so does $G(x, 0, z)$. Equation (4) can, hence, not be used. However, the case of size and shape fluctuations (§5) can be modified so as to be compatible with two-dimensional statistical homogeneity. Equation (6) then becomes

$$\begin{aligned} I(q_x, q_z) = {}& \int_{-\infty}^{\infty}\int_{-\infty}^{\infty} \mathrm{d}x\,\mathrm{d}z\, \exp[i(q_x x + q_z z)]\langle V(x, 0)\rangle \\ & \times \int_0^t \mathrm{d}z'\, \Omega(z + z')\Omega(z')G(x, 0, z, z'). \end{aligned} \tag{8}$$

For simplicity, we assumed that the film thickness is constant, *i.e.* $p(t) = \delta(t - \langle t \rangle)$. Thickness fluctuations can be taken into account but at the expense of a considerable increase in computing times[2] as mentioned earlier. It should be stressed that the displacement field induced by misfit dislocations has been derived by Kaganer *et al.* (1997) assuming a laterally infinite film. The existence of the $\Omega(x, 0)$ term violates this assumption. Equation (8) must hence be used carefully when dealing with misfit dislocations. In particular, the crystallites should be laterally much larger than the lateral extension of the strain field around a dislocation. Finally, equation (8) can be used to model RSMs of thin films containing strain gradients. In such a case, the pair correlation function $G(x, 0, z, z')$ contains a specific expression of the displacement profile, *e.g.* a polynomial or a power-law profile, or, as recently suggested (Boulle *et al.*, 2003), an adaptative profile based on cubic *B*-spline functions.

To illustrate the applicability of the approach presented, we calculate the RSM of the 200 reflection of a (100)-oriented yttria-stabilized zirconia (YSZ) film deposited onto (0001) sapphire. The film has been deposited by sol–gel dip coating followed by high-temperature thermal annealing treatments (1 h at 873 K and 1 h at 1773 K). Details concerning sample elaboration can be found elsewhere (Boulle, Guinebretière, Masson *et al.*, 2005). Atomic force microscopy (AFM) revealed that the film is made of roughly cylindrical islands with diameter ~150 nm and thickness ~20 nm. (200) and (400) RSMs were recorded with a high-resolution diffractometer allowing fast RSM acquisition (Boulle *et al.*, 2002; Masson *et al.*, 2005). IP (q_x) and OOP (q_z) line scans were extracted and analysed using the approach presented in this work. To perform the simulation, the cylinders were approximated with hexagonal prisms with a lognormal diameter PDF and a normal thickness PDF. The parameters obtained from this analysis were then used as input to calculate the RSM (Fig. 6). The agreement with the experimental RSM is very good which therefore validates the parameters obtained from the simulation of line scans. The diameter and thickness distribution are depicted in Figs. 6(*c*) and 6(*d*). The average island diameter is 127 nm and the square root of the variance of the diameter distribution is 18 nm. The average island thickness is 17 nm and the square root of the variance of the thickness distribution is 5 nm. These dimensions are in close agreement with AFM observations. A peculiarity of this sample is that it contains localized strain fields, *i.e.* distorted regions with limited spatial extension. This feature is responsible for the occurrence of a two-component intensity distribution made of a narrow coherent (Bragg) scattering peak and a broad diffuse scattering peak. The coherent peak (labelled C in Fig. 6) arises from long-range order inherent in crystalline materials (Krivoglaz, 1969) and its shape therefore only depends on size and shape effects. The coherent peak is streaked in the q_z direction because of the limited film thickness, whereas it is of limited extension in the q_x direction because of the larger dimensions of the crystallites in this direction. On the contrary, the diffuse peak (labelled D) depends on both size and disorder effects and it hence significantly extends in the q_x direction. Both features are clearly reproduced in the calculated RSM. For clarity, a q_x scan performed through the centre of the 200 and 400 reflections is also reported (Fig. 6*e*) together with calculated profiles. It must be emphasized that, contrary to size and shape effects, the effects of lattice disorder on the scattered intensity depend on the length of the

[2] Notice that equation (8) contains three integrals and that $G(x, 0, z, z')$ also implies a numerical evaluation in the case of low dislocation densities (Kaganer *et al.*, 1997). In the case of high dislocation densities, $G(x, 0, z, z') \approx G(x, 0, z)$ and one straightforwardly obtains equation (6).

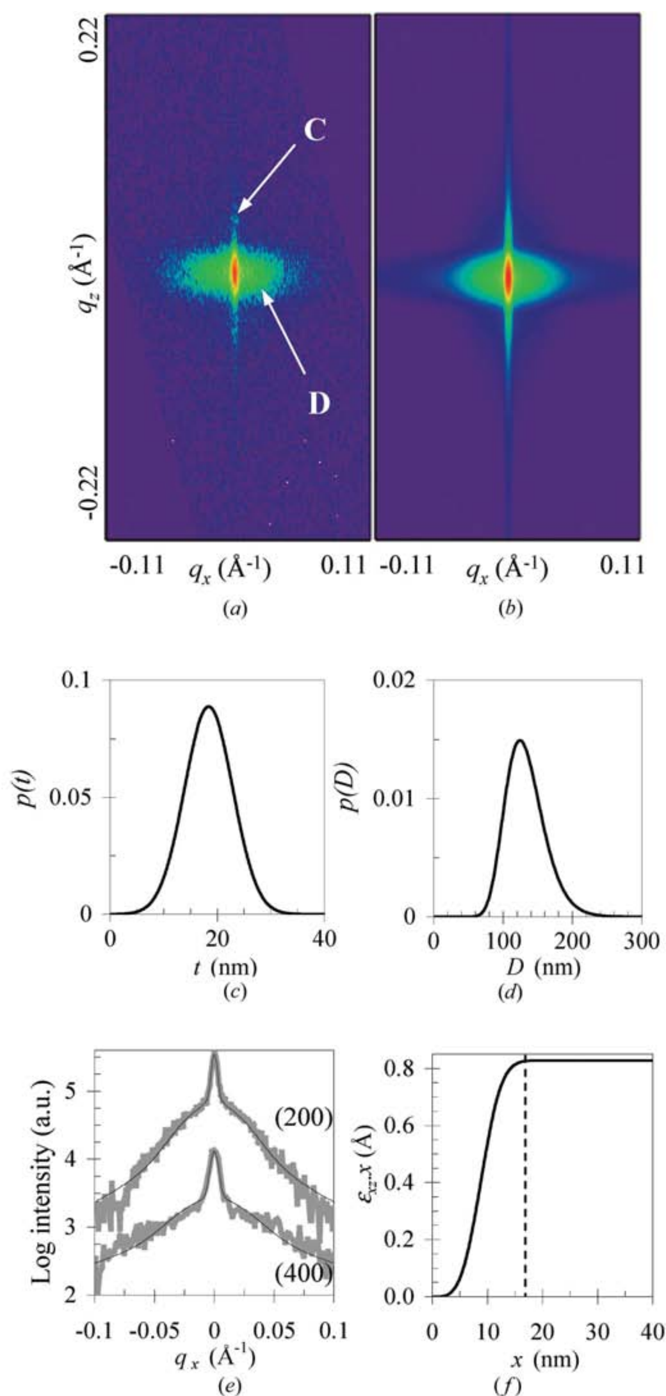

Figure 6
(*a*) Experimental and (*b*) calculated (200) RSM of a (100)-oriented YSZ film grown on (0001) sapphire. C and D denote the coherent and diffuse peak, respectively. (*c*) Crystallite thickness and (*d*) crystallite diameter distributions. The average thickness is 17 nm and the square root of the variance of the thickness distribution is 5 nm. The average diameter is 127 nm and the standard uncertainty of the diameter distribution is 18 nm. (*e*) Line (q_x) scan performed through the centre (q_z = 0) of the (200) (upper curve) and (400) (lower curve) reciprocal-lattice points. Grey line: experimental data, black line: model. (*f*) Plot of the lattice disorder function $\varepsilon_{xz}x$ *versus* the in-plane distance. For distances $x < 17$ nm, the displacements accumulate (left-hand side of the dashed line), whereas, for $x > 17$ nm, the displacements do not accumulate any more (right-hand side) and the disorder saturates to a constant value (*i.e.* the strain ε_{xz} decreases).

reciprocal-lattice vector **h**. It is therefore important to analyse (at least) two RSMs corresponding to different reciprocal-lattice vectors in order to recover the actual h dependence of lattice disorder effects. In the present case, the exact nature of the defect giving rise to the two-component profile is not known. To account for the existence of a two-component line profile, the effects of strain were hence described with the pair correlation function given by equation (7) and the strain component, ε_{xz}, was written in a functional form that includes a correlation length above which the lattice displacements do not accumulate any more, *i.e.* the strain drops to zero. It can be observed that both the 200 and 400 profiles are very well described with this model. The corresponding distribution of ε_{xz} is displayed in Fig. 6(*f*). It is striking to notice that the lattice displacements accumulate up to $x \simeq 17$ nm, which corresponds to the island thickness. Such a behaviour has already been reported for misfit dislocations in epitaxic thin films (Miceli *et al.*, 1996). Further details on that topic can be found elsewhere (Boulle, Guinebretière, Masson *et al.*, 2005; Boulle, Guinebretière & Dauger, 2005).

Finally, the resolution of the diffractometer can be straightforwardly incorporated in the analysis by convoluting the intensity distribution with the two-dimensional resolution function of the diffractometer, $R(q_x, q_z)$. Since equations (4) and (6) are two-dimensional Fourier transforms, this convolution is readily performed by multiplying the integrand of equations (4) and (6) with the Fourier transform of $R(q_x, q_z)$.

7. Conclusions

The crystalline domains over which diffraction is coherent (crystallites) in actual thin films are rarely of constant size and shape. We have presented an approach that allows size and shape fluctuations to be accounted for in the simulation of RSMs of epitaxic thin films. The derivation is carried out in the framework of the kinematical theory of diffraction. An important result is that the expression of the two-dimensional intensity distribution has the form of a two-dimensional Fourier transform whatever the case considered: constant size and shape, size fluctuations only, or size and shape fluctuations. Consequently, since the integrand of the Fourier integral has a simple analytical expression in all cases, there is no increase in computing times by taking size and shape fluctuations into account. The major assumptions made in the derivation are the same as those usually made (more or less implicitly) in the analysis of the defect structure of thin films by means of X-ray diffraction. Our approach is therefore compatible with most models of lattice disorder and should therefore be particularly useful for the analysis of imperfect thin-film structures which, in addition to significant lattice disorder, also exhibit crystallite size and shape fluctuations. Moreover, the instrumental resolution can be straightforwardly included in the analysis. The applicability of the model was tested with an epitaxic film of (100)-oriented YSZ made of cylindrical islands with fluctuating thickness and diameter and containing localized strain fields. A good agreement between the observed and the calculated RSM was obtained.

References

Authier, A. (2005). *Dynamical Theory of X-ray Diffraction*, *IUCr Monographs on Crystallography*, No. 11, reprinted with revisions. Oxford University Press.

Boulle, A., Guinebretière, R. & Dauger, A. (2005). *J. Appl. Phys.* **97**, 073503-1–8.

Boulle, A., Guinebretière, R., Masson, O., Bachelet, R., Conchon, F. & Dauger, A. (2005). *Appl. Surf. Sci.* In the press.

Boulle, A., Masson, O., Guinebretière, R., Lecomte, A. & Dauger, A. (2002). *J. Appl. Cryst.* **35**, 606–614.

Boulle, A., Masson, O., Guinebretière, R. & Dauger, A. (2003). *J. Appl. Cryst.* **36**, 1424–1431.

Feller, W. (1970). *An Introduction to Probability Theory and its Applications.* New York: Wiley.

Gleiter, H. (2000). *Acta Mater.* **48**, 1–29.

Holý, V., Li, J. H., Bauer, G., Schäffler, F. & Herzog, H. J. (1995). *J. Appl. Phys.* **78**, 5013–5021.

Holý, V., Wolf, K., Kastner, M., Stanzl, H. & Gebhardt, W. (1994). *J. Appl. Cryst.* **27**, 551–557.

James, R. W. (1967). *The Optical Principles of the Diffraction of X-rays.* London: G. Bell and Sons Ltd.

Kaganer, V. M., Köhler, R., Schmidbauer, M., Optiz, R. & Jenichen, B. (1997). *Phys. Rev. B*, **55**, 1793–1810.

Kaganer, V. M., Brandt, O., Trampert, A. & Ploog, K. H. (2005). *Phys. Rev. B*, **72**, 045423-1–12.

Kirste, L., Pavlov, K. M., Mudie, S. T., Punegov, V. I. & Herres, N. (2005). *J. Appl. Cryst.* **38**, 183–192.

Krivoglaz, M. A. (1969). *Theory of X-ray and Thermal Neutron Scattering by Real Crystals.* New York: Plenum.

Masson, O., Boulle, A., Guinebretière, R., Lecomte, A. & Dauger, A. (2005). *Rev. Sci. Instrum.* **76**, 063912-1–7.

Miceli, P. F., Wheatherwax, J., Krenstel, T. & Palmstrom, C. J. (1996). *Physica (Utrecht)*, B**221**, 230–234.

Nesterets, Y. I. & Punegov, V. I. (2000). *Acta Cryst.* A**56**, 540–548.

Nolan, J. P. (1998). *Stat. Prob. Lett.* **38**, 187–195.

Pietsch, U., Holý, V. & Baumbach, T. (2004). *High Resolution X-ray Scattering – from Thin Films to Lateral Nanostructures*, 2nd ed. New York: Springer Verlag.

Ratnikov, V., Kyutt, R., Shubina, T., Paskova, T., Valcheva, E. & Monemar, B. (2000). *J. Appl. Phys.* **88**, 6252–6252.

Scardi, P. & Leoni, M. (2001). *Acta Cryst.* A**57**, 604–613.

Schmidbauer, M. (2004). *X-ray Diffuse Scattering from Self-organized Mesoscopic Semiconductor Structures*, *Springer Tracts in Modern Physics*, Vol. 199. Berlin: Springer Verlag.

Thomson, C. V. (1990). *Ann. Rev. Mater. Sci.* **20**, 245–268.

Vargas, R., Louër, D. & Langford, J. I. (1983). *J. Appl. Cryst.* **16**, 512–518.

Warren, B. E. (1969). *X-ray Diffraction.* New York: Addison-Wesley.